Published in final edited form as:
Neuroscience. 2016 October 29; 335: 103–113. doi:10.1016/j.neuroscience.2016.08.026.

SEX-DEPENDENT MITOPHAGY AND NEURONAL DEATH FOLLOWING RAT NEONATAL HYPOXIA–ISCHEMIA

T. G. DEMAREST[a,d], **E. L. WAITE**[b], **T. KRISTIAN**[a,f], **A. C. PUCHE**[d,e], **J. WADDELL**[c], **M. C. MCKENNA**[c,d], and **G. FISKUM**[a,d,*]

[a]Department of Anesthesiology and the Center for Shock, Trauma, and Anesthesiology Research (S.T.A.R.), University of Maryland School of Medicine, Baltimore, MD 21201, USA

[b]Department of Chemistry and Biochemistry, University of Maryland, College Park, MD 21201, USA

[c]Department of Pediatrics, University of Maryland School of Medicine, Baltimore, MD 21201, USA

[d]Program in Neuroscience, University of Maryland School of Medicine, Baltimore, MD 21201, USA

[e]Department of Anatomy and Neurobiology, University of Maryland School of Medicine, Baltimore, MD 21201, USA

[f]Veterans Affairs Medical Center, University of Maryland School of Medicine, Baltimore, MD 21201, USA

Abstract

Males are more susceptible than females to long-term cognitive deficits following neonatal hypoxic-ischemic encephalopathy (HIE). Mitochondrial dysfunction is implicated in the pathophysiology of cerebral hypoxia–ischemia (HI), but the influence of sex on mitochondrial quality control (MQC) after HI is unknown. Therefore, we tested the hypothesis that mitophagy is sexually dimorphic and neuroprotective 20–24 h following the Rice–Vannucci model of rat neonatal HI at postnatal day 7 (PN7). Mitochondrial and lysosomal morphology and degree of co-localization were determined by immunofluorescence in the cerebral cortex. No difference in mitochondrial abundance was detected in the cortex after HI. However, net mitochondrial fission increased in both hemispheres of female brain, but was most extensive in the ipsilateral hemisphere of male brain following HI. Basal autophagy, assessed by immunoblot for the autophagosome marker LC3BI/II, was greater in males suggesting less intrinsic reserve capacity for autophagy following HI. Autophagosome formation, lysosome size, and TOM20/LAMP2 co-localization were increased in the contralateral hemisphere following HI in female, but not male brain. An accumulation of ubiquitinated mitochondrial protein was observed in male, but not female brain following HI. Moreover, neuronal cell death with NeuN/TUNEL co-staining occurred in both hemispheres of male brain, but only in the ipsilateral hemisphere of female brain after HI. In summary, mitophagy induction and neuronal cell death are sex dependent following HI. The deficit in elimination of damaged/dysfunctional mitochondria in the male brain following HI may

*Correspondence to: G. Fiskum, University of Maryland School of Medicine, 685 West Baltimore Street, Bldg. MSTF 5-34, Baltimore, MD 21201, USA. Fax: +1-410-706-2550. gfiskum@anes.umm.edu (G. Fiskum).

contribute to male vulnerability to neuronal death and long-term neurobehavioral deficits following HIE.

Keywords

mitophagy; sex-dependent; cell death; morphology; mitochondria; lysosome

INTRODUCTION

Neonatal hypoxic-ischemic encephalopathy (HIE) is a sexually dimorphic brain disorder affecting approximately 1.5–2/1000 live births (Kurinczuk et al., 2010; Davidson et al., 2015). Males are particularly vulnerable to adverse long-term outcome compared to females affected by HIE (Hill and Fitch, 2012; Smith et al., 2014), but sex-dependent pathophysiological mechanisms are not well understood. No sex differences in lesion volume have been found following HI in rats (Smith et al., 2014), but there is one recent report of increased lesion volume in male compared to female mice following HI (Mirza et al., 2015). Cell death proclivity in several brain injury models is sexually dimorphic (Du et al., 2004; Li et al., 2005, 2009, 2011; Yuan et al., 2009; Siegel et al., 2011; Manwani and McCullough, 2011; Hill et al., 2011a; Hill and Fitch, 2012; Siegel and McCullough, 2013) and a sex difference in cell death was also recently reported in moderate, but not severe hypoxia–ischemia (HI) injury in postnatal day 7 (PN7) rats (Askalan et al., 2015). The large body of clinical evidence demonstrating adult females have a better outcome after stroke than similarly aged males is commonly attributed to the presence of estrogen (reviewed in Turtzo and McCullough, 2010). In contrast, the mechanisms underlying neonatal sex differences in neurobehavioral outcome, when brain hormone levels are equivalent (Konkle and McCarthy, 2011), are not well understood. While hormone concentrations are similar, there is evidence that sex differences in androgen modulation of GABAergic neurotransmission may influence the susceptibility to neonatal brain injury (Nunez and McCarthy, 2008). Despite this growing evidence, sex differences in clinical studies of perinatal brain injury remain largely underrepresented.

It is well established that mitochondrial dysfunction and oxidative stress contribute to cell death following neonatal HI injury (Blomgren and Hagberg, 2006; Niatsetskaya et al., 2012; Ten and Starkov, 2012). We recently reported a male susceptibility to mitochondrial respiratory dysfunction and oxidative damage following HI (Demarest et al., 2016). These findings support the hypothesis that a mitochondrial mechanism may underlie the sex differences in long-term neurobehavioral outcome observed following HI. Mitochondrial fission (or fragmentation) (Pradeep et al., 2014; Zhang et al., 2015; Owens et al., 2015a) and autophagy (Weis et al., 2014; Li et al., 2015; Yu et al., 2015) are known to occur following cerebral ischemia–reperfusion injury. It is hypothesized that mitochondrial fragmentation segregates oxidatively modified mitochondrial proteins for elimination via mitochondrial-specific autophagy (mitophagy) (Twig et al., 2008; Soubannier et al., 2012; Norton et al., 2014). Increases in autophagy following ischemia–reperfusion injury are well recognized. However, there are conflicting reports that increased autophagy following cerebral ischemia-reperfusion injury can be detrimental (Baek et al., 2014; Yang et al., 2015; Au et al., 2015;

He et al., 2016; Xie et al., 2016) or neuroprotective (Carloni et al., 2012; Qi et al., 2014; Su et al., 2014; Wang et al., 2014; Jiang et al., 2015). Sex differences in autophagy both *in vitro* (Du et al., 2009) and *in vivo* following HI (Weis et al., 2014) have been reported. However, the role of mitophagy following neonatal HI is unknown. Thus, in the current study, we tested the hypothesis that mitophagy is sexually dimorphic and neuroprotective 20–24 h following neonatal HI.

EXPERIMENTAL PROCEDURES

Animals

All animal procedures were approved by the University of Maryland Institutional Animal Care and Use Committee in accordance with the NIH Guide for the Care and Use of Laboratory Animals. $N = 146$ total postnatal day 8 (PN8) Sprague–Dawley rat pups from timed pregnant females were obtained from Charles River Laboratories (Wilmington, MA) for this study. Of these, $n = 48$ male, and $n = 51$ females were used for 6–11 individual brain mitochondria isolations per group as previously described (Demarest et al., 2016). The remaining pups were allocated to the following groups for biochemical measures and histology: Sham $n = 10$ male, $n = 11$ female; HI: $n = 14$ male, $n = 12$ female. Some tissues used in this study were derived from the same cohort of animals used in a previous study (Demarest et al., 2016).

Western blot

Total brain homogenate (25 μg protein per sample) was subjected to sodium dodecyl sulfate-polyacrylamide gel electrophoresis (SDS–PAGE) using the BioRad tetra cell system and AnyKd® gels (BioRad, Hercules, CA, USA). Gels were transferred to 0.2 μm pore size PVDF via the Transblot Turbo semidry transfer system (BioRad). Blots were blocked in 5% milk in Tris-buffered saline (TBS) plus 0.1% tween-20 and incubated overnight at 4 °C with outer mitochondrial membrane marker TOM20 (1:2000; Santa Cruz, Dallas, TX, USA), autophagosome marker LC3BI/II (1:1000; Cell Signaling, Danvers, MA, USA) or β-actin (1:2000; Sigma, St. Louis, MO, USA) and washed 3 × 10 min in TBS plus 0.1% tween-20 (TBST) and incubated in goat anti-rabbit-HRP secondary (1:5000) in 5% milk in TBST. Blots were visualized using Amersham (GE healthcare, Little Chalfont, UK) chemiluminescent substrate and scanned for densitometry analysis on the Digit imaging system (LiCor, Lincoln, NE, USA). Densitometry was normalized to β-actin. $n = 4–6$/group.

Dot blot

Brain mitochondria were isolated from rat pups as previously described (Demarest et al., 2016). Isolated brain mitochondria (2.5 μg) were dotted onto nitrocellulose membrane using the Bio-Dot® SF Microfiltration Apparatus (BioRad) according to the manufacturer's instructions. Nitrocellulose membranes were blocked for 1 h in TBST+ 5% milk, washed in TBST and incubated in TBST+ 5% milk plus anti-ubiquitin antibody (1:1000; Cell Signaling) overnight at 4 °C, washed 6 × 10 min in TBS plus 0.1% tween-20 (TBST) and incubated in goat anti-rabbit-HRP secondary (1:10,000) in 5% milk in TBST. Blots were visualized with SuperSignal™ West Femto (ThermoFisher, Waltham, MA, USA) on BioRad

Chemidoc™ MP imaging system. The chemiluminescent signal was calculated in relative light units (RLU) per μg of protein. n = 6–11/group.

Fluorescence immunohistochemistry

Forty-micron thick brain sections were cut and mounted as previously described (Demarest et al., 2016). Following a thirty-minute permeabilization in TBS+ 0.03% Triton-X (TBSTx), sections were co-incubated in TOM20 (SantaCruz) and LAMP2 (SantaCruz) primary antibodies in IHC slide holders (Millipore, Billerica, MA, USA) for 72 h at 4 °C. Slides were washed in TBSTx 6 times for 10 min prior to a 72-h incubation with secondary antibodies; donkey anti-rabbit alexa 488 ReadyProbes® (Invitrogen, Carlsbad, CA, USA) and Donkey anti-Goat IgG (H + L), Alexa Fluor® 555 conjugate (ThermoFisher). Slides were removed from IHC slide Holders and washed in TBSTx 6 times for 10 min and cover-slipped using DAPI containing mounting media (DAPI Flouromount-G®; SouthernBiotech, Birmingham, AL, USA) prior to imaging. n = 4/group.

TOM20/LAMP2 image acquisition and analysis

Images were acquired at 63.3× oil magnification on a Zeiss Axioimager M2 microscope using the apotome. Images of three brain sections containing CA1 hippocampus were captured to ensure consistent cortical area between animals. Three images of cortical layers II/III per hemisphere, in each section, were imaged to ensure sufficient sampling of the cortex and eliminate any potential selection bias. A total of 9 images per hemisphere were acquired and analyzed for each animal. Particle size analysis and percent area (thresholds: 20–255 for TOM20, 30–255 for LAMP2) for each of the stained images were performed in Image J Software (National Institutes of Health). Analysis of the nine images per hemisphere was averaged per animal, resulting in n = 4 per group for statistical analysis. For LAMP2 staining, average particle size (μm^2) was calculated since there was a relatively small size distribution. For TOM20 size analysis, the large size distribution (from 0.2 to 100 μm^2) was determined by size distribution cumulative frequency analysis in bins of 0.1 μm^2 with a minimum size set at 0.2 μm^2. A total of 128,358 ± 10,693 (mean ± SD) TOM20-immunopositive particles were quantified per hemisphere in each brain assessed.

Mitochondria/lysosome colocalization

Mitochondrial (TOM20) and Lysosome (LAMP2) co-localization was calculated as percent of total cells displaying co-labeling (as defined by ⩾2 co-localized perinuclear puncta/cell). Fifteen-micrometer thick 3D z-stack images were captured with a 63.3× oil immersion objective and uploaded to Volocity software (PerkinElmer, Waltham, MA, USA) to validate that green/red co-labeling, signified by yellow fluorescence in the figures, was in fact co-localization in the 3D plane and not a super-positional artifact by proximity in different z-planes. A researcher blinded to experimental treatments counted total number of cells and cells with significant LAMP2/TOM20 co-labeling in nine 2D 63.3× images per hemisphere in each brain using Image J Cell Counter Analysis tool (NIH). DAPI-stained nuclei were counted, excluding edges, as a metric for total number of cells. Cells displaying co-labeling were counted simultaneously using a distinct marker. Counting was restricted to the perinuclear region to avoid false assignment of co-labeling to cells that may be in a different

z-plane. Equal numbers of cells were counted in each treatment group; 308 ± 22 cells (mean ± SD) were counted per hemisphere in each brain. $n = 4$ animals/group.

TUNEL staining

Following permeabilization in TBSTx, slide-mounted brain sections were placed in IHC slide holders (Millipore) and blocked in 2% horse serum (Invitrogen) for 2 h before overnight incubation in primary NeuN antibody (1:1000, Millipore). Slides were washed six times in TBSTx and incubated in donkey anti-mouse Alexa-594-conjugated secondary antibody (Invitrogen) for 2 h in the dark at room temperature. Following washing, TUNEL was detected with the Fluorescein In Situ Cell Death Detection (Roche, Basel, Switzerland) for 90 min in a humidified incubator at 37 °C. Neuronal cell death was quantified at 63.3 × magnification in ten randomly placed (100 μm × 125 μm) fields within the outlined cortex using the corpus callosum and perirhinal sulcus as anatomical boundaries. TUNEL/NeuN-positive cells were counted in three cortical brain sections using the unbiased optical fractionator probes in StereoInvestigator software (MBF Bioscience, Williston, VT). StereoInvestigator software uses the defined section thickness (z-stack) measured at each focal point, combined with the distance between serial sections (480 μm), to calculate total number of TUNEL/NeuN-positive neurons within that estimated volume. Coefficient of variation was 0.16 ± 0.07 (Mean ± SD) between groups. Cells were counted by an individual blinded to the identity of the animal treatment groups. $n = 4–5$/group.

Statistical analysis

No significant differences were found in any of the parameters studied between hemispheres in sham animals; thus sham hemispheres were combined for analysis ($n = 4–6$/group). Mitochondrial cumulative frequency size distribution analysis was performed using a custom Excel spreadsheet and nonparametric Kruskal-Wallace test with p-value adjusted for multiple comparisons. To determine statistically significant differences within distinct TOM20-immunopositive particle sizes, a two-way ANOVA was performed with Bonferroni's correction for multiple comparisons. For all other metrics, a two-way ANOVA (Sex × Treatment group; i.e., HI Contra, HI Ipsi, and Sham) was performed with Fisher's posthoc test. p-Values <0.05 were considered significant. All graphs were generated in Excel and reflect mean ± SEM.

RESULTS

Mitochondrial fragmentation

Mitochondria present within the brains of normal rats generally exhibit a tubular morphology. Under stress and/or pathological conditions, mitochondria can undergo rapid fission, which is often referred to as fragmentation (Owens et al., 2015). There were no significant differences in total number of TOM20 particles (Fig. 1C; $F(2,18) = 0.915$, $p = 0.9596$) or TOM20 immunoreactivity by western blot (Fig. 1E). However, the average TOM20 particle size (Fig. 1A, D; $F(2,18) = 9.159$, $p = 0.0018$) and percent mitochondrial area (Fig. 1B; $F(2, 18) = 6.699$, $p = 0.0067$) were significantly decreased in the ipsilateral cortex of both sexes following HI.

Mitochondrial cumulative size distribution analysis

Mitochondria are dynamic organelles which constantly change size via fusion and fission. To better understand the changes in average size, we determined the cumulative size distribution in each treatment group. Kruskal–Wallace nonparametric analysis revealed that the mitochondrial size distributions following HI were significantly different from sham (Fig. 2). Both sexes displayed a left shift in the curve, in both contralateral and ipsilateral hemispheres after HI, indicating greater numbers of smaller mitochondria, or increased net mitochondrial fragmentation/fission (Fig 2.). Further analysis of the size distributions revealed significant changes in distinct size ranges within the entire mitochondrial population (Table 1; $F(997, 17{,}964) = 531.1$, $p < 0.0001$). There was a significant increase in mitochondria (1.0–4.3 μm^2) in the contralateral hemisphere of male brain compared to sham (Table 1). There was a dramatic increase in fragmentation in >96% (0.2–18.2 μm^2 vs. sham) of the mitochondrial population in the ipsilateral hemisphere of the male brain following HI (Table 1). The mitochondria in the ipsilateral hemisphere of males had a significant increase in the number of smaller mitochondria, ranging in size from 0.2 to 11.1 μm^2 compared to the contralateral hemisphere. In the female brain, there were significantly more of the smallest mitochondria, ranging from 0.2 to 5.4 μm^2 and 0.2 to 10.5 μm^2 in the contralateral and ipsilateral hemispheres, respectively, following HI compared to sham animals. There was a significantly greater population of smaller mitochondria in the ipsilateral hemisphere compared to the contralateral hemisphere (0.2–4.4 μm^2) of the female brain following HI. More mid-sized mitochondria (1.2–6.2 μm^2) were found in the ipsilateral hemisphere of the male brain compared to the ipsilateral hemisphere of the female brain following HI (Table 1). There was a significant sex × treatment group interaction ($F(5, 17{,}964) = 1226$, $p < 0.001$). These observations suggest that mitochondrial fission is increased following HI, and that the degree of fission events occurring in male and female brain after injury differs.

Sex differences in autophagy

Mitochondrial fission is necessary for the targeted degradation of mitochondria by autophagy (mitophagy) (Frank et al., 2012; Zuo et al., 2014). To test the hypothesis that the degree of mitochondrial fragmentation correlates with increases in autophagy, we assessed autophagosome formation by LC3BI/II immunoblot (Fig. 3). There was significantly more autophagosome marker LC3BII immunoreactivity in sham males compared to sham females (Fig. 3). However, there were no changes in LC3BII levels following HI in males ($F(2, 21) = 0.2424$, $p = 0.7869$). In contrast, a significant increase in LC3BII levels was observed in the contralateral hemisphere of females following HI (Fig. 3; $F(2, 21) = 3.052$, $p = 0.042$). This observation suggests that autophagosome formation may be at maximal capacity in the male PN8 brain, thus limiting the ability of the male brain to upregulate autophagy in response to stress/injury.

Sex-dependent changes in lysosome morphology

The completion of autophagy relies on the fusion of autophagosomes with lysosomes, forming autolysosomes, for lysosomal degradation of proteins, lipids, and organelles. To determine whether increases in autophagosome formation parallel increases in autolysosome

formation, we assessed lysosome morphology by lysosome-associated membrane protein 2 (LAMP2) immunofluorescence. Lysosome particle analysis revealed no significant difference in the number of lysosomes in any treatment group (Fig. 4A. $F(2,31) = 1.575$, $p = 0.226$). There were no differences in LAMP2 particle size or percent area in male brain following HI. There were no significant differences in either size or percent area in the ipsilateral hemisphere of the female brain following HI. In contrast, we found significant increases in average LAMP2 particle size (Fig. 4A, C) and percent area (Fig. 4A, D) in the contralateral hemisphere of female brain following HI compared to sham females (Fig. 4A, C, D; $F(2,31) = 3.087$, $p = 0.017$). These increases in female brain were significantly greater than the average particle size and percent area observed in the contralateral hemisphere of the male brain after HI (Fig. 4A, C, D). These observations indicate that autophagosomes may be fusing with lysosomes, forming autolysosomes.

Sex-dependent induction of mitophagy following HI

To determine whether the increase in LAMP2 particle size reflects an increase in mitophagy, we determined the degree of colocalization of LAMP2/TOM20 by double-labeling immunofluorescence. The percentage of total cells displaying LAMP2/TOM20 co-labeling was significantly higher in the contralateral hemisphere of female brains following HI (Fig. 5A, B; $F(2,31) = 6.681$, $p = 0.011$). This increase in LAMP2/TOM20 co-labeling was significantly greater than that observed in the contralateral hemisphere of male brains following HI (Fig. 5A, B). In contrast, there was a significant decrease in LAMP2/TOM20 co-labeling in the ipsilateral hemisphere of male brains following HI (Fig. 5A, B, $p = 0.042$). The same statistical outcome was found with the raw number of cells observed in each treatment group (Fig. 5D). No difference in the total number of cells counted from equal fields of view was observed (Fig. 5E; $F(2,31) = 1.679$, $p = 0.206$). Additionally, there was a significant increase in ubiquitinated mitochondrial protein in the male brain following HI (Fig. 5C; ($F(2, 44) = 10.010$, $p < 0.001$). There was no change in mitochondrial protein ubiquitination in the female brain following injury. These observations suggest an increase in mitophagy in the contralateral hemisphere of females following HI, and an accumulation of damaged (ubiquitinated) mitochondrial protein in the male brain after HI.

Sex differences in neuronal cell death

In order to test the hypothesis that the increase in mitophagy is neuroprotective, we determined the amount of neuronal cell death by TUNEL/NeuN double-labeling immunofluorescence at 24 h following HI. There was no significant cell death in the contralateral hemisphere of the female brain following HI, in comparison to shams ($F(1,25) = 1.691$, $p = 0.207$). However, there was a significant increase in total (Fig. 6A, B) and neuronal (Fig. 6A, D) TUNEL-positive cells in the contralateral hemisphere of male brain following HI compared to shams (Fig. 6A, B; $F(1,25) = 9.235$, $p = 0.006$). The total number of TUNEL-positive cells in the contralateral hemisphere of male brain was significantly greater than in the contralateral hemisphere of female brain following HI (Fig. 6A, B; $F(1,25) = 5.319$, $p = 0.031$). A significant increase in total (Fig. 6B; $F(1,25) = 26.009$, $p < 0.001$) and neuronal (Fig. 6D; $F(1,25) = 11.445$, $p = 0.004$) cell death was observed in the ipsilateral hemisphere of both sexes following HI. Taken together, these data indicate that male brains are more sensitive to neuronal loss following injury.

DISCUSSION

In the current study, we present the first evidence for a sexually dimorphic induction of mitophagy (Figs. 4 and 5) and sex differences in neuronal cell death (Fig. 6) in the contralateral hemisphere 20–24 h after HI at PN7. We also determined that mitochondrial fragmentation occurs in contralateral and ipsilateral hemispheres, to differing degrees, in both sexes (Table 1; Figs. 1 and 2). Basal autophagy is higher in male brain compared to female brain in shams, (Fig. 3) and mitophagy is increased following HI in female, but not male brain (Fig. 5.) Moreover, the induction of mitophagy was associated with less neuronal death after HI (Fig. 6). This is the first report of significant cell death in the contralateral hemisphere, changes in mitochondria/lysosome morphology, and mitophagy following HI. These results support the hypothesis that mitochondrial quality control (MQC) is sexually dimorphic following HI, and may play a role in the sexually dimorphic neurobehavioral outcome of HI.

Sex differences in mitophagy

We observed more autophagosome marker LC3II in male sham vs. female sham suggesting a higher rate of constitutive autophagy in the male brain than female brain in PN8 rat pups (Fig. 3). Given that autophagosome formation in female brain increased to a similar degree as that observed in male shams, it is possible that the autophagy machinery in male brain is working at maximum capacity, and therefore cannot adapt to eliminate damaged cellular components following injury. This potential limitation might be the result of greater basal oxidative stress in the male PN8 brain, thus necessitating a higher turnover of proteins compared to the female brain. This relationship is supported by our previous observation that glutathione is 30% higher in PN8 female compared to male brains and may partially explain the accumulation of oxidatively damaged proteins in the male, but not female brain after HI (Demarest et al., 2016).

The results of the present study indicate a significant sexually dimorphic induction of mitophagy (Fig. 5) following HI. The induction of mitophagy is concomitant with significant increases in the smallest mitochondria (0.2–5.4 μm^2) (Fig. 2, Table 1) and is associated with less neuronal cell death (Fig. 6), suggesting a neuroprotective role for mitophagy in the female brain following HI. Mitochondrial fission is hypothesized to segregate oxidatively damaged mitochondrial components into smaller mitochondrial fragments that are targeted to autophagosomes for fusion with lysosomes and degradation via mitophagy (Twig et al., 2008;Soubannier et al., 2012; Norton et al., 2014). Mitochondrial fragmentation is a common observation following cerebral ischemia–reperfusion injury in adult rodents (Pradeep et al., 2014; Zhang et al., 2015; Owens et al., 2015b).

Sex differences in mitochondria/lysosome morphology

Mitochondrial fragmentation is mediated by a family of fission proteins including dynamin-related protein (Drp1). Drp1 is required for mitochondrial fragmentation such that inhibition of Drp1 with siRNA results in accumulation of damaged mitochondria by selectively blocking autophagy (Zuo et al., 2014). These results suggest that mitochondrial fragmentation is essential to eliminate damaged/dysfunctional mitochondria via mitophagy

following ischemic brain injury. Our observations that mitochondria in the contralateral hemisphere of the female brain fragment into the smallest sizes (0.2 μm^2) (Fig. 2, Table 1), together with an increase in lysosome size (Fig. 4C, D); support the idea that autophagosome–lysosome fusion occurs to promote mitophagy in the female brain following HI. There is also a more extensive accumulation of mid-sized mitochondrial fragments (1.2–6.2 μm^2) (Fig. 2, Table 1) in the ipsilateral hemisphere of male brain compared to the female brain following HI. Additionally, there is a significant decrease in TOM20/LAMP2 co-labeling in the ipsilateral hemisphere of male brain (Fig 6B). While these observations are limited to 20–24 h following HI, and we cannot exclude the possibility that mitophagy may occur at an earlier time point, the accumulation of ubiquitinated mitochondrial proteins (Fig. 6C) suggests that autophagy/mitophagy is impaired in the male brain following HI. Indeed, inhibition of mitochondrial fission results in increased protein oxidation and increased lesion volume following middle cerebral artery occlusion (MCAO) in adult male rats (Zuo et al., 2014). Therefore, impaired mitophagy may contribute to the increase in oxidatively damaged proteins and mitochondrial dysfunction observed in the male brain compared to the female brain following HI (Demarest et al., 2016).

We previously reported a male-specific susceptibility to impaired mitochondrial complex I-mediated respiration in the contralateral hemisphere following HI (Demarest et al., 2016). These findings, taken together with our current observations suggest that clearance of damaged mitochondria in the contralateral hemisphere of the female brain may contribute to the sparing of complex I-mediated respiration after HI. These results are in agreement with the previously mentioned studies demonstrating increases in autophagy following cerebral ischemia in adult (Qi et al., 2014; Su et al., 2014; Wang et al., 2014; Jiang et al., 2015), and in neonatal rats following HI (Weis et al., 2014). However, Weis et al. (2014) speculated that accumulation of the autophagosome marker LC3BII following HI in the female brain is due to a deficit in autophagosome–lysosome fusion. However, the increase in lysosome size observed in the present study is consistent with the fusion of lipid bound vesicles that occurs during autolysosome formation. Increased mitochondrial/lysosome co-localization further suggests that mitophagy occurs in the female brain after injury. Moreover, our results suggest that increased mitophagy is associated with decreased neuronal cell death.

Sex-dependent neuronal death following HI

Cell death following HI is described as a continuum of apoptosis and necrosis (Northington et al., 2007). The contralateral hemisphere, exposed to hypoxia, is often used for normalization of ipsilateral lesion volume (Nijboer et al., 2007; Fan et al., 2013) and not assessed for cell death (Carloni et al., 2012; Thatipamula et al., 2015; Li et al., 2016). Studies from our group (Waddell et al., 2016; Demarest et al., 2016; Xu et al., 2015) and others (Smith et al., 2016) clearly demonstrate that neuropathology occurs in the contralateral side of brain after HI. Until recently, there have been no reported sex differences in lesion volume or magnitude of cell death following HI. Thus far, there has been one report of decreased lesion volume in female mice compared to males 3 days post-injury (Mirza et al., 2015), and only one report of increased cell death in the male brain at 7 days post-injury that is dependent on moderate injury severity (Askalan et al., 2015). The lack of consistent sex differences in histopathology is likely due to differences in species,

severity of injury, and time point post-injury. These inconsistent findings have led some to conclude that the sex difference in neurobehavioral outcome is the result of a sex-dependent plasticity or compensatory mechanism (Smith et al., 2014; Cohen and Stonestreet, 2014). Results of the current study showing upregulation of mitophagy, coupled with our previous results demonstrating the female brain is able to upregulate glutathione peroxidase activity following HI are consistent with sex-dependent compensatory mechanisms (Demarest et al., 2016).

Sex differences in behavioral outcome following HI are most likely due to a combination of compensatory mechanisms and sexually dimorphic cell death proclivity (reviewed in Hill and Fitch, 2012; Demarest and McCarthy, 2015). In the current study, we observed a slight, but significant, increase in neuronal cell death in the contralateral hemisphere of the male, but not female, brain following HI (Fig. 6). Our data are consistent with the recent report from Waddell et al. (2016) who observed a significant reduction in hippocampal volume in the contralateral hemisphere of male brain 33 days after HI at PN10 (Waddell et al., 2016). Smith et al. (2016) also observed an increased contralateral hippocampal volume in females compared to males after HI (Smith et al., 2016). Taken together, these results suggest that the male brain is more susceptible to the hypoxia–reperfusion component of HI injury than the female brain. The sexually dimorphic cell death pathways (reviewed in (Hill and Fitch, 2012; Demarest and McCarthy, 2015) likely play a role in the female resilience to hypoxia–reperfusion injury. The female cell death proclivity for caspase-dependent cell death, combined with their higher levels of intrinsic X-linked Inhibitor of apoptosis (XIAP) protein (Hill et al., 2011b), an endogenous caspase inhibitor, may account for the relative resilience of the female brain to hypoxia–reperfusion injury. On the other hand, male cell death proclivity for PARP-1/AIF-mediated cell death may contribute to mitochondrial dysfunction in male brain after HI as PARP-1 activation contributes to mitochondrial dysfunction. Further study is needed to parse out the sex-dependent relationship between cell death pathway proclivity and MQC. Collectively, our results suggest that deficits in mitophagy, mitochondrial dysfunction, and oxidative stress contribute to male susceptibility to hypoxia-mediated injury.

CONCLUSIONS

In summary, the present study suggests the female brain has an innate ability to upregulate mitophagy, which protects the contralateral hemisphere from neuronal cell death. These findings, in conjunction with other studies, lead us to hypothesize that the induction of autophagy/mitophagy may be another component of sex-specific compensatory mechanisms to prevent the accumulation of oxidatively damaged cellular components, protect against mitochondrial dysfunction, and attenuate cell death following neonatal HI. These results contribute to the understanding of sex-dependent pathophysiological mechanisms of HI injury, and subsequent endogenous neuroprotective mechanisms, which will aid in the development of new therapeutic targets for infants suffering from HIE.

Abbreviations

HI hypoxia–ischemia

HIE	hypoxic-ischemic encephalopathy
LAMP2	lysosome-associated membrane protein 2
LC3BI/II	microtubule-associated proteins 1A/1B light chain 3B
MCAO	middle cerebral artery occlusion
MQC	mitochondrial quality control
PN	postnatal day
TOM20	translocase of outer membrane 20
TUNEL	terminal deoxynucleotidyl transferase dUTP nick end labeling

References

Askalan R, Gabarin N, Armstrong EA, Fang LY, Couchman D, Yager JY. Mechanisms of neurodegeneration after severe hypoxic-ischemic injury in the neonatal rat brain. Brain Res. 2015; 1629:94–103. [PubMed: 26485031]

Au AK, Chen Y, Du L, Smith CM, Manole MD, Baltagi SA, Chu CT, Aneja RK, Bayir H, Kochanek PM, Clark RS. Ischemia-induced autophagy contributes to neurodegeneration in cerebellar Purkinje cells in the developing rat brain and in primary cortical neurons in vitro. Biochim Biophys Acta. 2015; 1852:1902–1911. [PubMed: 26071643]

Baek SH, Noh AR, Kim KA, Akram M, Shin YJ, Kim ES, Yu SW, Majid A, Bae ON. Modulation of mitochondrial function and autophagy mediates carnosine neuroprotection against ischemic brain damage. Stroke. 2014; 45:2438–2443. [PubMed: 24938837]

Blomgren K, Hagberg H. Free radicals, mitochondria, and hypoxia-ischemia in the developing brain. Free Radical Biol Med. 2006; 40:388–397. [PubMed: 16443153]

Carloni S, Buonocore G, Longini M, Proietti F, Balduini W. Inhibition of rapamycin-induced autophagy causes necrotic cell death associated with Bax/Bad mitochondrial translocation. Neuroscience. 2012; 203:160–169. [PubMed: 22209856]

Cohen SS, Stonestreet BS. Sex differences in behavioral outcome following neonatal hypoxia ischemia: Insights from a clinical meta-analysis and a rodent model of induced hypoxic ischemic injury. Exp Neurol. 2014; 256:70–73. [PubMed: 24726666]

Davidson JO, Wassink G, van den Heuij LG, Bennet L, Gunn AJ. Therapeutic hypothermia for neonatal hypoxic-ischemic encephalopathy – Where to from here? Front Neurol. 2015; 6:198. [PubMed: 26441818]

Demarest TG, McCarthy MM. Sex differences in mitochondrial (dys)function: implications for neuroprotection. J Bioenerg Biomembr. 2015; 47:173–188. [PubMed: 25293493]

Demarest TG, Schuh RA, Waddell J, McKenna MC, Fiskum G. Sex-dependent mitochondrial respiratory impairment and oxidative stress in a rat model of neonatal hypoxic-ischemic encephalopathy. J Neurochem. 2016; 137:714–729. [PubMed: 27197831]

Du L, Bayir H, Lai Y, Zhang X, Kochanek PM, Watkins SC, Graham SH, Clark RS. Innate gender-based proclivity in response to cytotoxicity and programmed cell death pathway. J Biol Chem. 2004; 279:38563–38570. [PubMed: 15234982]

Du L, Hickey RW, Bayir H, Watkins SC, Tyurin VA, Guo F, Kochanek PM, Jenkins LW, Ren J, Gibson G, Chu CT, Kagan VE, Clark RS. Starving neurons show sex difference in autophagy. J Biol Chem. 2009; 284:2383–2396. [PubMed: 19036730]

Fan X, van BF, van der Kooij MA, Heijnen CJ, Groenendaal F. Hypothermia and erythropoietin for neuroprotection after neonatal brain damage. Pediatr Res. 2013; 73:18–23. [PubMed: 23085819]

Frank M, Duvezin-Caubet S, Koob S, Occhipinti A, Jagasia R, Petcherski A, Ruonala MO, Priault M, Salin B, Reichert AS. Mitophagy is triggered by mild oxidative stress in a mitochondrial fission dependent manner. Biochim Biophys Acta. 2012; 1823:2297–2310. [PubMed: 22917578]

He G, Xu W, Tong L, Li S, Su S, Tan X, Li C. Gadd45b prevents autophagy and apoptosis against rat cerebral neuron oxygen-glucose deprivation/reperfusion injury. Apoptosis. 2016; 21:390–403. [PubMed: 26882903]

Hill CA, Fitch RH. Sex differences in mechanisms and outcome of neonatal hypoxia-ischemia in rodent models: implications for sex-specific neuroprotection in clinical neonatal practice. Neurol Res Int. 2012; 2012:867531. [PubMed: 22474588]

Hill CA, Alexander ML, McCullough LD, Fitch RH. Inhibition of X-linked inhibitor of apoptosis with embelin differentially affects male versus female behavioral outcome following neonatal hypoxia-ischemia in rats. Dev Neurosci. 2011a; 33:494–504. [PubMed: 22041713]

Hill CA, Alexander ML, McCullough LD, Fitch RH. Inhibition of X-linked inhibitor of apoptosis with embelin differentially affects male versus female behavioral outcome following neonatal hypoxia-ischemia in rats. Dev Neurosci. 2011b; 33:494–504. [PubMed: 22041713]

Jiang T, Yu JT, Zhu XC, Zhang QQ, Tan MS, Cao L, Wang HF, Shi JQ, Gao L, Qin H, Zhang YD, Tan L. Ischemic preconditioning provides neuroprotection by induction of AMP-activated protein kinase-dependent autophagy in a rat model of ischemic stroke. Mol Neurobiol. 2015; 51:220–229. [PubMed: 24809692]

Konkle AT, McCarthy MM. Developmental time course of estradiol, testosterone, and dihydrotestosterone levels in discreteregions of male and female rat brain. Endocrinology. 2011; 152:223–235. [PubMed: 21068160]

Kurinczuk JJ, White-Koning M, Badawi N. Epidemiology of neonatal encephalopathy and hypoxic-ischaemic encephalopathy. Early Hum Dev. 2010; 86:329–338. [PubMed: 20554402]

Li H, Pin S, Zeng Z, Wang MM, Andreasson KA, McCullough LD. Sex differences in cell death. Ann Neurol. 2005; 58:317–321. [PubMed: 15988750]

Li L, Tan J, Miao Y, Lei P, Zhang Q. ROS and autophagy: interactions and molecular regulatory mechanisms. Cell Mol Neurobiol. 2015; 35:615–621. [PubMed: 25722131]

Li Y, Liu K, Kang ZM, Sun XJ, Liu WW, Mao YF. Helium preconditioning protects against neonatal hypoxia-ischemia via nitric oxide mediated up-regulation of antioxidases in a rat model. Behav Brain Res. 2016; 300:31–37. [PubMed: 26675888]

Liu F, Li Z, Li J, Siegel C, Yuan R, McCullough LD. Sex differences incaspase activation after stroke. Stroke. 2009; 40:1842–1848. [PubMed: 19265047]

Liu F, Lang J, Li J, Benashski SE, Siegel M, Xu Y, McCullough LD. Sex differences in the response to poly(ADP-ribose) polymerase-1 deletion and caspase inhibition after stroke. Stroke. 2011; 42:1090–1096. [PubMed: 21311064]

Manwani B, McCullough LD. Sexual dimorphism in ischemic stroke: lessons from the laboratory. Womens Health (Lond Engl). 2011; 7:319–339. [PubMed: 21612353]

Mirza MA, Ritzel R, Xu Y, McCullough LD, Liu F. Sexually dimorphic outcomes and inflammatory responses in hypoxic-ischemic encephalopathy. J Neuroinflamm. 2015; 12:32.

Niatsetskaya ZV, Sosunov SA, Matsiukevich D, Utkina-Sosunova IV, Ratner VI, Starkov AA, Ten VS. The oxygen free radicals originating from mitochondrial complex I contribute to oxidative brain injury following hypoxia-ischemia in neonatal mice. J Neurosci. 2012; 32:3235–3244. [PubMed: 22378894]

Nijboer CH, Groenendaal F, Kavelaars A, Hagberg HH, van BF, Heijnen CJ. Gender-specific neuroprotection by 2-iminobiotin after hypoxia-ischemia in the neonatal rat via a nitric oxide independent pathway. J Cereb Blood Flow Metab. 2007; 27:282–292. [PubMed: 16736041]

Northington FJ, Zelaya ME, O'Riordan DP, Blomgren K, Flock DL, Hagberg H, Ferriero DM, Martin LJ. Failure to complete apoptosis following neonatal hypoxia-ischemia manifests as "continuum" phenotype of cell death and occurs with multiple manifestations of mitochondrial dysfunction in rodent forebrain. Neuroscience. 2007; 149:822–833. [PubMed: 17961929]

Norton M, Ng AC, Baird S, Dumoulin A, Shutt T, Mah N, Andrade-Navarro MA, McBride HM, Screaton RA. ROMO1 is an essential redox-dependent regulator of mitochondrial dynamics. Sci Signal. 2014; 7:ra10. [PubMed: 24473195]

Nunez JL, McCarthy MM. Androgens predispose males to GABAA-mediated excitotoxicity in the developing hippocampus. Exp Neurol. 2008; 210:699–708. [PubMed: 18289534]

Owens K, Park JH, Gourley S, Jones H, Kristian T. Mitochondrial dynamics: cell-type and hippocampal region specific changes following global cerebral ischemia. J Bioenerg Biomembr. 2015; 47:13–31. [PubMed: 25248415]

Pradeep H, Sharma B, Rajanikant GK. Drp1 in ischemic neuronal death: an unusual suspect. Curr Med Chem. 2014; 21:2183–2189. [PubMed: 24372214]

Qi Z, Yan F, Shi W, Zhang C, Dong W, Zhao Y, Shen J, Ji X, Liu KJ, Luo Y. AKT-related autophagy contributes to the neuroprotective efficacy of hydroxysafflor yellow A against ischemic stroke in rats. Transl Stroke Res. 2014; 5:501–509. [PubMed: 24804941]

Siegel CS, McCullough LD. NAD+ and nicotinamide: sex differences in cerebral ischemia. Neuroscience. 2013; 237:223–231. [PubMed: 23403179]

Siegel C, Li J, Liu F, Benashski SE, McCullough LD. MiR-23a regulation of X-linked inhibitor of apoptosis (XIAP) contributes to sex differences in the response to cerebral ischemia. Proc Natl Acad Sci U S A. 2011; 108:11662–11667. [PubMed: 21709246]

Smith AL, Alexander M, Rosenkrantz TS, Sadek ML, Fitch RH. Sex differences in behavioral outcome following neonatal hypoxia ischemia: Insights from a clinical meta-analysis and a rodent model of induced hypoxic ischemic brain injury. Exp Neurol. 2014

Smith AL, Rosenkrantz TS, Fitch RH. Effects of sex and mild intrainsult hypothermia on neuropathology and neural reorganization following neonatal hypoxic ischemic brain injury in rats. Neural Plast. 2016; 2016:2585230. [PubMed: 27042359]

Soubannier V, McLelland GL, Zunino R, Braschi E, Rippstein P, Fon EA, McBride HM. A vesicular transport pathway shuttles cargo from mitochondria to lysosomes. Curr Biol. 2012; 22:135–141. [PubMed: 22226745]

Su J, Zhang T, Wang K, Zhu T, Li X. Autophagy activation contributes to the neuroprotection of remote ischemic perconditioning against focal cerebral ischemia in rats. Neurochem Res. 2014; 39:2068–2077. [PubMed: 25082119]

Ten VS, Starkov A. Hypoxic-ischemic injury in the developing brain: the role of reactive oxygen species originating in mitochondria. Neurol Res Int. 2012; 2012:542976. [PubMed: 22548167]

Thatipamula S, Al RM, Zhang J, Hossain MA. Genetic deletion of neuronal pentraxin 1 expression prevents brain injury in a neonatal mouse model of cerebral hypoxia-ischemia. Neurobiol Dis. 2015; 75:15–30. [PubMed: 25554688]

Turtzo LC, McCullough LD. Sex-specific responses to stroke. Future Neurol. 2010; 5:47–59. [PubMed: 20190872]

Twig G, Elorza A, Molina AJ, Mohamed H, Wikstrom JD, Walzer G, Stiles L, Haigh SE, Katz S, Las G, Alroy J, Wu M, Py BF, Yuan J, Deeney JT, Corkey BE, Shirihai OS. Fission and selective fusion govern mitochondrial segregation and elimination by autophagy. EMBO J. 2008; 27:433–446. [PubMed: 18200046]

Waddell J, Hanscom M, Shalon EN, McKenna MC, McCarthy MM. Sex differences in cell genesis, hippocampal volume and behavioral outcomes in a rat model of neonatal HI. Exp Neurol. 2016; 275(Pt 2):285–295. [PubMed: 26376217]

Wang P, Xu TY, Wei K, Guan YF, Wang X, Xu H, Su DF, Pei G, Miao CY. ARRB1/beta-arrestin-1 mediates neuroprotection through coordination of BECN1-dependent autophagy in cerebral ischemia. Autophagy. 2014; 10:1535–1548. [PubMed: 24988431]

Weis SN, Toniazzo AP, Ander BP, Zhan X, Careaga M, Ashwood P, Wyse AT, Netto CA, Sharp FR. Autophagy in the brain of neonates following hypoxia-ischemia shows sex- and region-specific effects. Neuroscience. 2014; 256:201–209. [PubMed: 24184979]

Xie C, Ginet V, Sun Y, Koike M, Zhou K, Li T, Li H, Li Q, Wang X, Uchiyama Y, Truttmann AC, Kroemer G, Puyal J, Blomgren K, Zhu C. Neuroprotection by selective neuronal deletion of Atg7 in neonatal brain injury. Autophagy. 2016; 12:410–423. [PubMed: 26727396]

Xu S, Waddell J, Zhu W, Shi D, Marshall AD, McKenna MC, Gullapalli RP. In vivo longitudinal proton magnetic resonance spectroscopy on neonatal hypoxic-ischemic rat brain injury: Neuroprotective effects of acetyl-L-carnitine. Magn Reson Med. 2015; 74:1530–1542. [PubMed: 25461739]

Yang X, Hei C, Liu P, Song Y, Thomas T, Tshimanga S, Wang F, Niu J, Sun T, Li PA. Inhibition of mTOR Pathway by Rapamycin Reduces Brain Damage in Rats Subjected to Transient Forebrain Ischemia. Int J Biol Sci. 2015; 11:1424–1435. [PubMed: 26681922]

Yu J, Bao C, Dong Y, Liu X. Activation of autophagy in rat brain cells following focal cerebral ischemia reperfusion through enhanced expression of Atg1/pULK and LC3. Mol Med Rep. 2015; 12:3339–3344. [PubMed: 26018745]

Yuan M, Siegel C, Zeng Z, Li J, Liu F, McCullough LD. Sex differences in the response to activation of the poly (ADP-ribose) polymerase pathway after experimental stroke. Exp Neurol. 2009; 217:210–218. [PubMed: 19268668]

Zhang XM, Zhang L, Wang G, Niu W, He Z, Ding L, Jia J. Suppression of mitochondrial fission in experimental cerebral ischemia: the potential neuroprotective target of p38 MAPK inhibition. Neurochem Int. 2015; 90:1–8. [PubMed: 26116440]

Zuo W, Zhang S, Xia CY, Guo XF, He WB, Chen NH. Mitochondria autophagy is induced after hypoxic/ischemic stress in a Drp1 dependent manner: the role of inhibition of Drp1 in ischemic brain damage. Neuropharmacology. 2014; 86:103–115. [PubMed: 25018043]

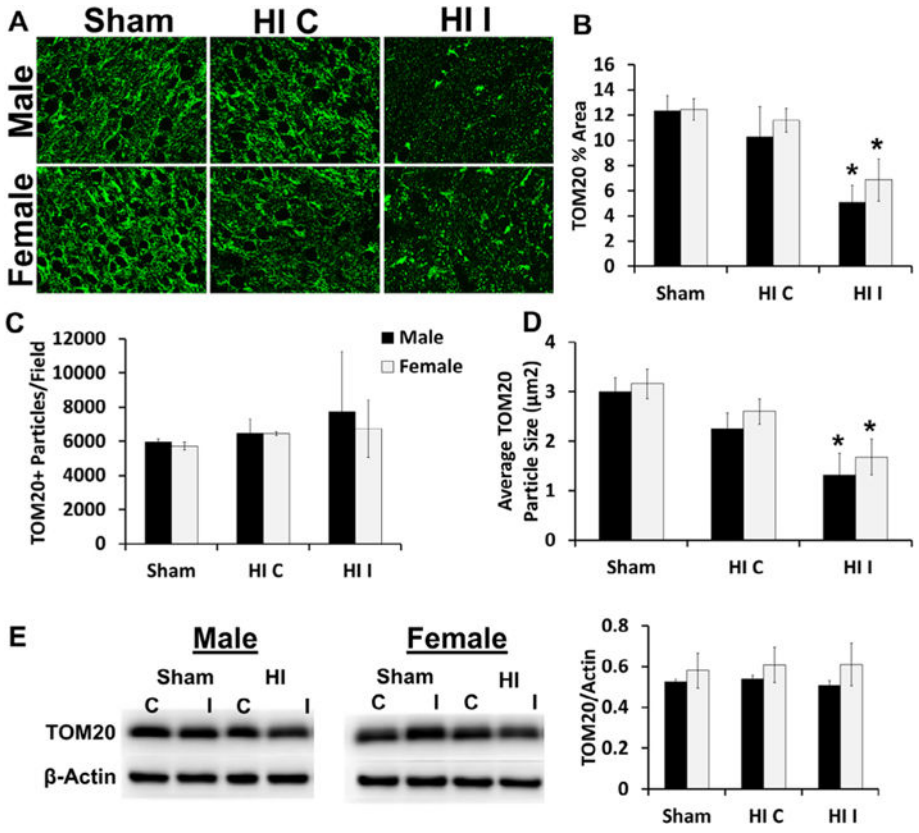

Fig. 1.

Mitochondrial fragmentation following neonatal HI. (A) Representative images of mitochondrial morphology in sham (left), HI Contra (HI C; middle) and HI Ipsi (HI I; right) of male (top) and female (bottom) cortex. (B) Decreased average percent field of view covered by TOM20 + mitochondria following HI in both sexes. (C) No difference in the average number of TOM20 + mitochondrial particles per field (D) Significant decrease in the average size of TOM20 mitochondrial particles (n = 4/group). (E) No difference in total brain homogenate TOM20 immunoreactivity (n = 6/group). *$p < 0.05$ vs. sham. Bars reflect mean ± SEM.

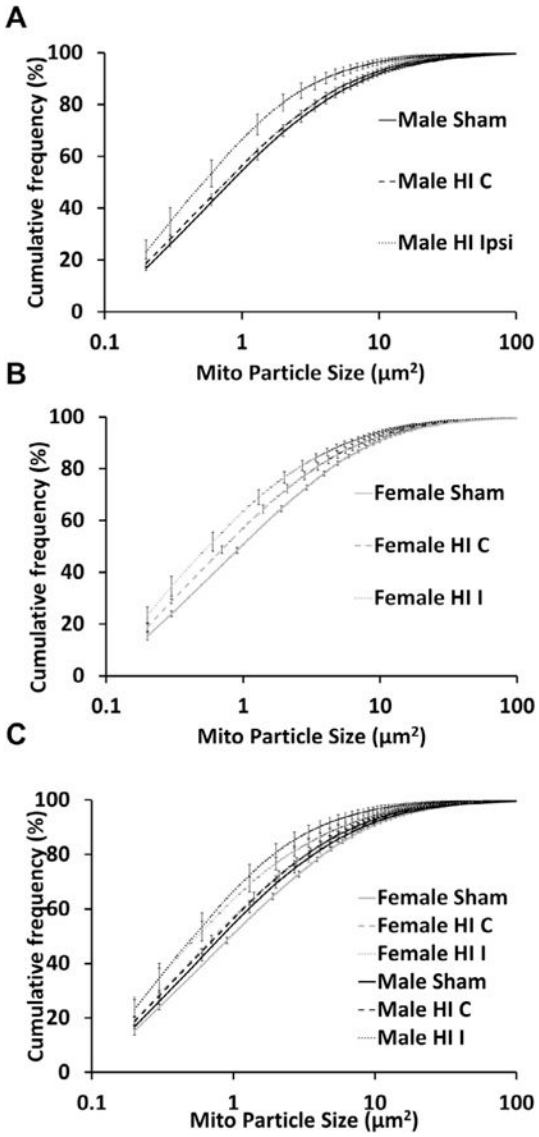

Fig. 2.

Mitochondria size distribution cumulative frequency analysis. Cumulative frequency curves of cortical brain mitochondria particle size (μm^2) of male (A) and female (B) rat pups following HI. (C) Sex and treatment size distribution comparison. A total of 128,358 ± 10,693 (mean ± SD) mitochondria were analyzed per hemisphere ($n = 4$/group). Kruskal–Wallace nonparametric analysis with p-values adjusted for multiple comparisons indicated all curves are significantly left shifted vs. sham ($p < 0.01$) indicative of an increase in mitochondrial fragmentation. Bars reflect mean ± SEM.

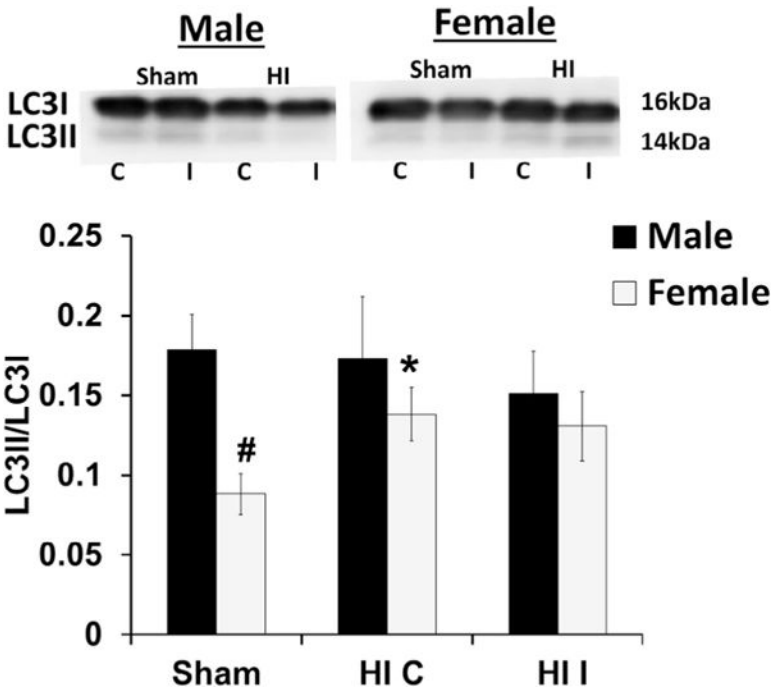

Fig. 3.

Sex differences in autophagosome formation. Densitometry of LC3II/LC3I revealed a significant sex difference ($^{\#}p < 0.05$) in total brain homogenate of sham animals and a significant increase ($^{*}p < 0.05$) in the contralateral hemisphere of female, but not male, brain following HI vs. sham ($^{*}p < 0.05$). $n = 6$/group. Bars reflect mean ±SEM.

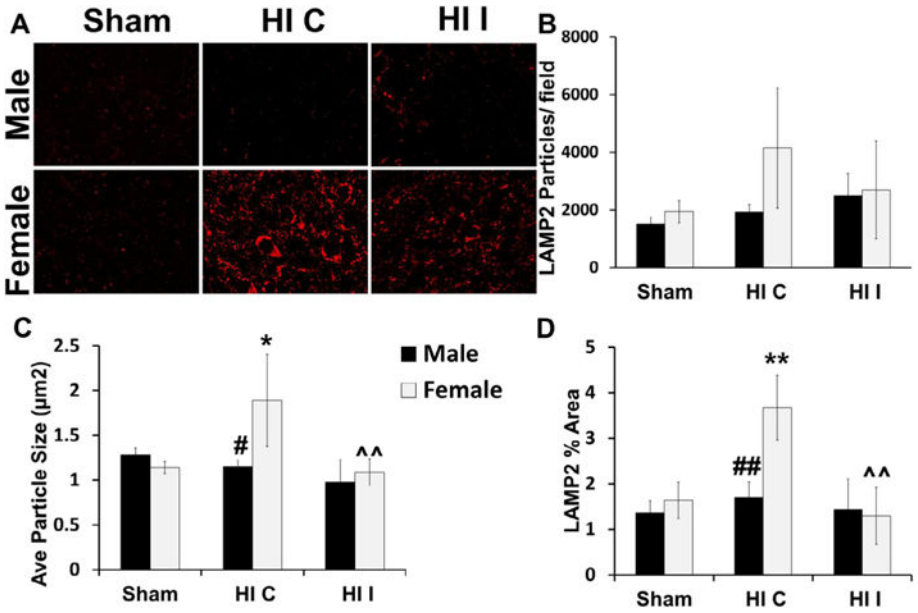

Fig. 4.

Sex-dependent changes in lysosome morphology following neonatal HI. (A) Representative images of lysosome morphology in sham (left), HI Contra (HI C; middle), and HI Ipsi (HI I; right) of male (top) and female (bottom) cortex. (B) No difference in the average number of particles per field. Significant increases in average particle size (C) and average percent field of view (D) covered by LAMP2 + lysosomes in the contralateral hemisphere of female brain following HI. $^{*}p < 0.05$, $^{**}p < 0.01$ vs. sham. $^{\#}p < 0.05$, $^{\#\#}p < 0.01$ vs. other sex. $n = 4$/group. Bars reflect mean ± SEM.

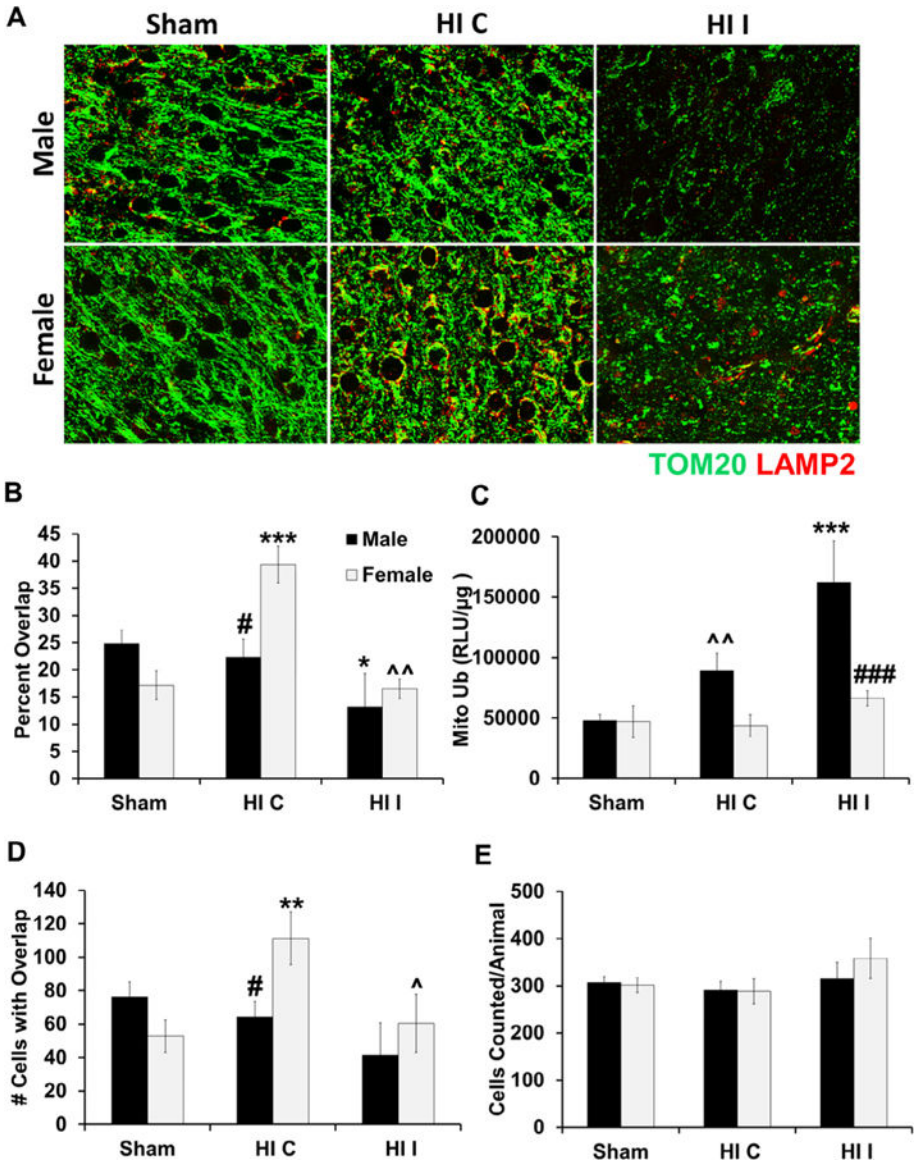

Fig. 5.

Sexually dimorphic induction of mitophagy following HI. (A) Representative images of mitochondria/lysosome co-labeling in sham (left), HI Contra (HI C; middle), and HI Ipsi (HI I; right) of male (top) and female (bottom) cortex. A significant increase in TOM20/LAMP2 co-labeling occurs in the contralateral hemisphere of the female (B), but not male (D), brain after HI ($n = 4$/group). (C) Ubiquitination of mitochondrial proteins accumulates in the male brain following HI ($n = 6$/group). *$p < 0.05$, **$p < 0.01$, ***$p < 0.001$ vs. sham. $p < 0.05$, $p < 0.01$ vs. other hemisphere. $^{\#}p < 0.05$, $^{\#\#\#}p < 0.001$ vs. other sex. There is a significant (sex × treatment group) interaction $p = 0.012$, 0.017 for percent cells with co-labeling and number of total cells with co-labeling, respectively. Bars reflect mean ± SEM.

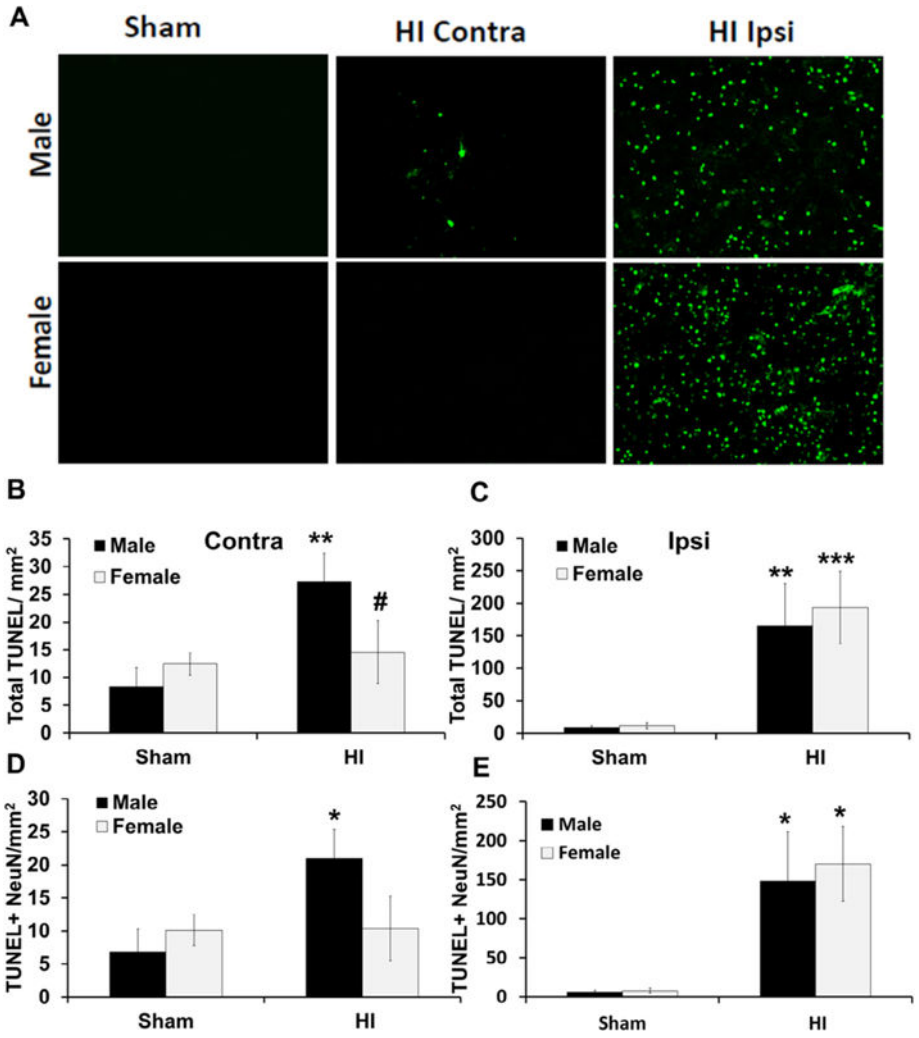

Fig. 6.

Sex differences in cell death following HI. Representative images of NeuN+ neurons (red) and TUNEL+ cells (green) in sham (left), HI Contra (HI C; middle), and HI Ipsi (HI I; right) of male (top) and female (bottom) cortex. A significant increase in neuronal cell death occurs in the contralateral hemisphere of male, but not female, brain following HI (B, D). Significant neuronal cell death is observed in the ipsilateral hemisphere of both sexes following HI (C, E). $*p < 0.05$, $**p < 0.01$, $***p < 0.001$ vs. sham. $^{\#}p < 0.05$ vs. other sex. $n = 4–5$/group. Bars reflect mean ± SEM. (For interpretation of the references to color in this figure legend, the reader is referred to the web version of this article.)

Table 1

Significant fragmentation within specific mitochondrial size ranges. Analysis of the entire mitochondrial size distributions by a two-way ANOVA and Bonferroni correction for multiple comparisons determined significant differences between groups compared (left column) within a specific size range (middle column) of the mitochondrial population at the significance levels depicted (right column). ns = non-significant

	Mito size range (μm^2)	**Significance**
Male		
Sham vs HI C	1.0–4.3	$p < 0.01$–0.05
Sham vs. HI I	0.2–18.2	$p < 0.0001$–0.05
HI C vs. HI I	0.2–11.1	$p < 0.0001$–0.05
Female		
Sham vs. HI C	0.2–5.4	$p < 0.0001$–0.05
Sham vs. HI I	0.2–10.5	$p < 0.0001$–0.05
HI C vs. HI I	0.2–4.4	$p < 0.0001$–0.05
Male vs. female		
Male Sham vs. female sham		ns
Male HI C vs. female HI C		ns
Male HI I vs. female HI I	1.2–6.2	$p < 0.01$–0.05